Light absorption by brown carbon in the Southeastern United States is pH dependent

Sabrina M. Phillips, Aleia D. Bellcross, Geoffrey D. Smith*

Department of Chemistry, University of Georgia, 140 Cedar St Athens, GA 30602 USA

* corresponding author: Department of Chemistry, University of Georgia, 140 Cedar St Athens, GA 30602 USA, phone: 706-583-0478, fax: 706-542-9454, e-mail: gsmith@chem.uga.edu

Abstract

Light-absorbing organic material, or "brown carbon" (BrC), can significantly influence the effect that aerosols have on climate. Here, we investigate how changing pH affects absorption spectra of water-soluble BrC from ambient particulate matter smaller than 2.5 μm collected in Athens, Georgia in Spring and Fall of 2016 including samples from nearby wildfires. We find that absorption increases 10% per pH unit from pH = 2 to pH = 12 with a broad, featureless tail at visible wavelengths where the largest fractional increase is also observed. The resulting change in the spectral shape causes the absorption Ångström exponent to decrease by 0.18 per unit increase in pH. Similar behavior with humic substances suggests that they and BrC share a common link between pH and absorption, which we propose could be a consequence of conformational changes in supramolecular assemblies thought to exist in humic substances. Specifically, we hypothesize that a wider variety and larger number of absorbing charge transfer complexes are formed as functional groups in these molecules, such as carboxylic acid and phenol moieties, become deprotonated. These findings suggest that: 1) the pH of ambient particulate matter samples should be measured or controlled, and 2) radiative forcing by BrC aerosols could be overestimated if their pH dependent BrC absorption is not accounted for in models.

1. Introduction

Atmospheric aerosols affect radiative forcing both directly through their interaction with sunlight as well as indirectly through their influence on clouds. It is clear that black carbon (BC) particles are very efficient absorbers of solar radiation, with some evaluations suggesting that its impact on radiative forcing is second only to carbon dioxide among anthropogenic forcing agents.[1] However, the role of organic carbon (OC) is much less well understood, and many climate models ignore light absorption by this fraction even though it has recently become clear that some OC does absorb light. This light-absorbing fraction, sometimes called "brown carbon" (BrC), generally has an absorption spectrum that varies much more strongly with wavelength than BC does. As a consequence, BrC is not believed to contribute substantially to aerosol absorption past 500 nm, though at UV wavelengths it can be comparable to BC[2] and can decrease OH production by up to 30%.[3]

There is substantial evidence that this BrC can originate from biomass burning,[4-8] and many laboratory studies have also elucidated mechanisms for the creation of light-absorbing organic species from aqueous reactions of small ketones and aldehydes with amines and ammonium salts[9-12] and the formation of N-heterocycles[13], amines,[14] and secondary imines (Schiff bases).[15] However, the identification of specific chromophores in samples of ambient particulate matter has proven difficult, as discussed by Laskin et al.[16] and references therein. Some studies have isolated nitrophenols as an important class of chromophores, though these have only accounted for 4% of measured BrC absorption.[17-19] Lin et al. were able to attribute as much as 25% of solvent-extractable absorption to nitrophenols and their derivatives and another 25% to PAH derivatives in particulate matter collected from controlled combustion of various biofuels,[13] and Desyaterik et al. attributed 48% of absorption in collected cloud water samples impacted by biomass burning to a collection of nitrophenols and aromatic carbonyls.[17] Phillips and Smith have also found that as much as 50% of water-extracted BrC absorption from ambient samples can be attributed to charge transfer complexes formed through the interaction

between aromatic carbonyl species and phenolic species[20,21] in analogy to terrestrial and aquatic humic substances.[22,23]

Without a more complete molecular characterization of the organic molecules constituting BrC, it is difficult to predict how its absorption spectrum might evolve in the atmosphere. For example, it may change as the particles photochemically age, the chromophores photobleach, the identities and concentrations of inorganic salts in the particles change, or the pH of the particles changes. The effect of pH, in particular, could be important as it is known to influence the physical and optical properties of humic substances,[24-29] which some fractions of ambient aerosol are known to resemble.[30] Despite the fact that estimates of aerosol pH vary from 0 to 9 in atmospheric particles,[31-35] the effect of pH changes on BrC absorption has not been studied very much at all, and most studies do not measure, much less control, the pH of solvent-extracted filter samples. Lee et al.[36] did find an increase in absorption with increasing pH of water extracts of laboratory-generated naphthalene secondary organic aerosols, which they attributed to deprotonation of nitrophenols. Phillips and Smith[20] demonstrated a similar increase for water-extracted ambient particulate matter noting the similarities with humic substances.[23] Likewise, Teich et al.[37] very recently reported a 60% increase in 370 nm absorption of water-soluble ambient filter extracts when pH increased from 2 to 10, but there is no indication of how pH affects absorption at other wavelengths or pH values, and no physicochemical explanation for the effect was offered. In none of these studies was the role of pH the central focus.

Here, we systematically examine the effect of changing pH on the magnitude and spectral shape of UV-visible absorption by water-soluble ambient brown carbon. We draw on observed similarities with the pH dependent absorption of humic substances to motivate a few plausible explanations including a link between structural changes induced by changing pH and observed absorption changes. We also explore the potential impacts of the pH dependence for the climate through simplified estimates of radiative forcing efficiency.

2. Materials and Methods

2.1 *Aerosol and fulvic acid samples*

Ambient aerosols were collected out of a window in the Chemistry Building at the University of Georgia (~20 m above ground level) in Athens, Georgia (33.9488°N, 83.3747°W), during the months of April, August, September, October, and November of 2016, including five days when the air quality in Athens, GA was heavily impacted by nearby forest fires burning over 100,000 acres across the Southeastern United States.[38] A total of 15 samples (10 baseline ambient, five wildfire) were collected on 47 mm diameter polytetrafluoroethylene (PTFE, Teflon) filters (0.2 μm pore size, Sterlitech) at 16.7 L/min. for separate periods ranging from 24 hours to 168 hours (7 hours - 48 hours for days influenced by the wildfires). Details of the individual samples are given in Table S1 in the Supplementary Information. The baseline ambient samples represent those collected on days for which no visible smoke was evident and when few wildfires were active in the Southeast U.S. according to Moderate Resolution Imaging Spectroradiometer (MODIS) fire count maps obtained from the NASA Earthdata Worldview website. [39] The Hybrid Single Particle Lagrangian Integrated Trajectory Model (HYSPLIT) [40] was used to calculate back trajectories and confirm that sampled air masses had traveled through areas containing wildfires within 48 hours prior to sample collection. An example of a MODIS fire count map overlayed with a HYSPLIT back trajectory map for November 10, 2016 (a sample impacted by wildfires) is given in Figure S1 in the Supplementary Information.

A Very Sharp Cut Cyclone inlet (BGI, Inc.) with a stated d_{50} of 2.5 μm and a sharpness value ($(d_{16}/d_{84})^{½}$) of 1.16 at a flow rate of 16.7 L/min. was employed to size select for PM2.5 particles. Water-soluble organic species were extracted, similarly to Hecobian et al.,[41] by sonication of the filter for 20 min in 10 mL of Milli-Q water (<18.2 MΩ·cm). Extracted solutions were filtered using a 13 mm, 0.45 μm PTFE disposable syringe filter (VWR 28145-493). Suwannee River Fulvic Acid (SRFA) was purchased from the International Humic Substances Society and used without further purification or treatment. Solutions of SRFA in Milli-Q water were made at concentrations of 5 mg/L and 50 mg/L.

2.2 *pH measurement and adjustment*

The pH of each aqueous sample was measured using a pH meter (Omega, PHH222) with a gel-filled electrode (Omega, PHE-1332), which were calibrated daily with buffer solutions of pH = 4.01, 7.00, and 10.01. The initial pH of the baseline ambient samples taken before any adjustments were made was 4.20 (± 0.38), while the initial pH of the wildfire samples was 4.55 (± 0.41). The initial pH of the SRFA samples was 3.90. The pH was continuously monitored in the 1 cm cuvette during titration.

The pH of extracts in the cuvette was adjusted through the addition of 1-5 µl of HCl or NaOH solutions of 0.01, 0.1, or 1 M concentration using a micropipette. To minimize hysteresis effects[42,43] the solution pH was cycled between 2 and 11 prior to analysis. The pH was adjusted in increments of approximately one pH unit in both the forward (increasing pH) and the backward (decreasing pH) directions, and the aqueous solutions were stirred continuously using a small magnetic stir bar.

2.3 *Measurement of UV-visible spectra*

UV-visible absorption spectra (200 – 800 nm) of the aqueous extracts were measured on a Cary 60 UV−vis spectrophotometer (Agilent). The absorption spectra were fit to a power law function over the range 300-500 nm according to:

$$A(\lambda) = a \cdot \lambda^{-AAE} \quad (1)$$

where A is absorbance, a is a scaling constant, and AAE is the Absorption Ångström Exponent, which describes the wavelength dependence.

3. Results

3.1 *Water-soluble BrC absorption increases at all wavelengths with increasing pH*

The absorption spectra of water-soluble (WS) BrC (Figure 1) exhibit featureless, near-exponential shapes. There is a clear increase in absorption at all wavelengths as pH increases, yet the shapes of the spectra remain largely the same. Specifically, they all display a power law dependence on wavelength (Equation 1) for wavelengths greater than 300 nm, as illustrated by the linearly decaying absorption displayed on the log-log plot in the inset to Figure 1. The systematic increase in absorption with pH is more clearly evident in the plot of normalized integrated absorption (300-500 nm) vs. pH in Figure 2. Here, the integrated absorption of each spectrum has been normalized to the value at pH = 2 for the respective filter sample. For filters for which no measurement was made at pH = 2, we interpolated or extrapolated to pH = 2 from values at nearby pH's. This normalization allows the general trend of absorption with pH to be compared regardless of filter-to-filter variability in absorbance intensity and chromophore concentrations. On average, an increase of one unit in pH results in a 10% increase in integrated absorption. However, the samples clearly fall into two groups, with one showing a more pronounced pH dependence (with a 13% increase per pH unit) and the other a smaller one (with a 8% increase per pH unit), and in fact these slopes are statistically different at the $p < 0.01$ level. These groups may represent particles from different sources or of different photochemical age, but without chemical markers it is difficult to know.

Interestingly, we found that the magnitude of absorption from the wildfire samples also increased with pH (orange open circles in Figure 2) with a dependence resembling the upper group of baseline ambient samples (blue squares in Figure 2) that were not influenced by wildfire events (as determined from MODIS fire counts and HYSPLIT back trajectory calculations). The similarity hints at a possible correlation, perhaps indicating that some of what we have classified as baseline ambient samples might have originated from wildfire events further away, though we stress that this is very speculative. The spectra from the wildfire samples (Figure S2) are not fit well by a power law function, however, and demonstrate spectral features not evident in the baseline ambient samples. Also of note, the pH dependence of SRFA spectra (gray open triangles in Figure 2) is similar to the lower group of ambient

144 samples (green squares in Figure 2) suggesting a potential resemblance between these samples and humic
145 substances. The increase in absorption with pH observed in all samples suggests that this might be a
146 feature common to ambient WS BrC spanning a wide range of sources and photochemical age.

147 3.2 *Effect of pH on absorption is a function of wavelength*

148 While increasing pH increases WS BrC absorption at all wavelengths, the magnitude of this
149 increase was found to be a function of wavelength. Specifically, absorption at longer wavelengths
150 increases proportionately more than at shorter wavelengths. This trend is clear in Figure 3a in which the
151 ratio of the average absorption at pH = 5, 7, and 10 relative to absorption at pH = 2 is plotted. The
152 calculated ratio gets rather noisy at about 500 nm since the WS BrC spectra are very close to the detection
153 limit at this point. By way of comparison, Teich et al. report an increase in BrC absorption at 370 nm by
154 a factor of 1.6 in going from pH = 2 to pH = 10 in Germany;[37] here, we observe an increase by a factor of
155 2.0 at the same wavelength. The spectra of the SRFA demonstrate a very similar dependence on pH and
156 wavelength (Figure 3b), but with the larger signal-to-noise the trend is seen to persist to wavelengths up
157 to at least 700 nm. Previous work with SRFA and other humic and fulvic substances have also reported
158 more pronounced increase in absorption with increasing pH at longer wavelengths.[44,45]

159 The absorption ratio for both the WS BrC and the SRFA samples never falls below a value of
160 unity as would be expected if chromophores were removed due to deprotonation. For example, the 350
161 nm absorption peak of 4-nitrocatechol, a chromophore sometimes attributed to BrC,[19,46,47] disappears as
162 pH is raised above its first pKa of 6.65[48] while another peak at 425 nm, corresponding to the deprotonated
163 form, appears (see Figure S3). Any similar shifts in absorption occurring in the WS BrC samples would
164 have to be coincidentally compensated for by shifts associated with other chromophores to explain the
165 increase observed at all wavelengths. The unlikeliness of this coincidence occurring in all samples
166 suggests the existence of some other pH-dependent mechanism that affects the whole host of
167 chromophores. One such potential explanation involves the alteration of supramolecular assemblies of
168 molecules[49,50] and is discussed in more detail in section 4.

169 The wavelength dependence of the pH effect on absorption results in a subtle yet measurable
170 effect on the shape of the spectrum. As illustrated by the linear trends in the log-transformed spectra
171 shown in the Figure 1 inset, a power law function fits the spectra well, though the corresponding AAE
172 (reflected by the slope) does change. This trend is apparent in Figure 4 in which the AAE values from the
173 power law fits are plotted as a function of pH. Each sample exhibits this decrease in AAE individually
174 (shown in Figure S4), and on average the AAE decreases by 0.18 per unit pH increase. This systematic
175 relationship between AAE and pH is also observed with the SRFA samples, which demonstrate a similar
176 decrease of 0.16 per unit increase in pH, though the AAE's are on average 8% lower than for the WS
177 BrC. This similarity in the pH dependence of the spectral shapes further supports a common underlying
178 chemical explanation.

179 3.3 *Difference spectra reveal absorption features accompanying pH increase*

180 To better resolve changes in spectral features associated with changing pH, we used difference
181 absorbance spectroscopy (DAS). The DAS spectrum is calculated according to the equation:

182 $$\Delta A_{pH}(\lambda) = A_{pH}(\lambda) - A_{pH\_ref}(\lambda) \quad (2)$$

183 where $\Delta A_{pH}(\lambda)$ is the difference between the absorbance, A , at a particular value of pH and at a
184 reference pH, *pH_ref*. Here, *pH_ref* was chosen to be pH = 2, the lowest pH studied. Because DAS
185 isolates differences in absorbance spectra, it is useful for detecting subtle changes accompanying
186 changing physicochemical conditions; for example, it has been employed to investigate how absorption
187 by humic and fulvic substances and dissolved organic matter are affected by pH.[29,51] That work has
188 identified different DAS spectra at low pH values (pH < 6) and at high values (pH > 7) leading to the
189 suggestion that the observed changes are correlated with the deprotonation of carboxylic acids at low pH
190 and of phenols at high pH. These functional groups have previously been identified as being prevalent in
191 humic and fulvic substances with effective pKa's of 2.0 – 3.8 and 7.2 – 10.9 for carboxylic acids and

192 phenols, respectively.[52] Similarly, carboxylic acids have been found to account for 10% – 40% of organic
193 particulate matter from a variety of sources[53] and phenols arise from lignin burning and have been
194 identified in ambient and biomass burning aerosols.[13,16,54,55]

195 The average DAS spectra (Figure 5) were calculated by first normalizing each individual DAS
196 spectrum to the value at 370 nm and pH = 11; this was necessary to account for differences in magnitude
197 of absorption from day to day amongst the samples. These DAS spectra reflect the increase in overall
198 absorption with increasing pH observed in the spectra (Figure 1), but they also make it possible to
199 identify specific bands that appear and grow as pH increases such as the peaks near 260 nm and 300 nm.
200 It is possible that the peak at 260 nm could arise from aromatic species, which are known constituents of
201 humic substances and humic-like substances in particulate matter,[30] and absorb near this wavelength. For
202 example, benzene and many substituted benzene species have absorption peaks in the 250 nm – 270 nm
203 range.[56] Likewise, the peak near 300 nm could originate from phenolate anions created from the
204 deprotonation of phenol and substituted phenols; for example, the phenol absorption peak shifts from 270
205 nm to 287 nm upon deprotonation.[56] The 300 nm peak can be seen to grow in intensity relative to the 260
206 nm peak at pH = 7 and higher, precisely in the range of pKa's found for phenols in fulvic acids (pKa =
207 7.2 – 10.9 [52]).

208 The DAS spectra in Figure 5 also display what appears to be a broad continuum at wavelengths
209 longer than 350 nm. This band decreases monotonically with increasing wavelength while the magnitude
210 of absorption increases with pH at all wavelengths. Even more intriguing, this band looks nearly identical
211 for all pH values when normalized to the value at 370 nm at each pH (Figure 6a). Such normalization
212 makes it possible to view the spectral changes at different wavelengths relative to one another despite the
213 different magnitudes in the DAS spectrum at different pH values. It is clear that the shape of the
214 difference spectrum, that is how much absorption increases with pH as a function of wavelength, does not
215 change over the wide range of pH's from pH = 3 to pH = 11. By contrast, the relative magnitudes of the
216 peaks near 250 nm and 290 nm decrease dramatically with increasing pH. This behavior indicates that

217 there is something about the increasing pH that systematically increases absorption at $\lambda > 350$ nm in a
218 similar manner whether pH increases from 2 to 3 or from 2 to 11. This behavior is not consistent with a
219 simple model of a superposition of chromophores that are deprotonated at successively higher pH values
220 since that would involve a decrease in absorption by the chromophore at some wavelength accompanying
221 an increase in absorption by the deprotonated form at another. In fact, no decrease is observed at any
222 wavelengths over the entire range from 225 nm to 525 nm. Interestingly, the very same behavior is
223 observed at wavelengths longer than 350 nm in the normalized DAS spectra of SRFA (Figure 6b). For
224 both systems to demonstrate such a response to pH simply because of deprotonation of a superposition of
225 many chromophores would have to be highly coincidental. Instead, we interpret the similarity as further
226 support for a common explanation in which the increased absorption with increasing pH by both ambient
227 BrC and SRFA is attributed to a structural alteration of the aggregation of organic molecules. We discuss
228 this hypothesis in more detail in section 4.

229

230 **4. Discussion**

231 The systematic absorption increase with increasing pH observed in all ambient samples, including those
232 affected by wildfires, as well as humic substances, suggests an underlying chemical cause linked to
233 deprotonation. Elucidating this cause could be important for understanding how BrC absorption changes
234 as particle composition evolves in the atmosphere, how to compare disparate BrC measurements made at
235 a variety of sites with different sampling approaches and under different conditions, and how radiative
236 transfer in the atmosphere is sensitive to the pH of particles. Despite the clear link between pH and BrC
237 absorption, however, there is relatively little known about the chemical nature of this link. We believe
238 that there are likely several explanations for why absorption increases with increasing pH, including both
239 direct deprotonation of chromophores as well indirect modification of chromophores through structural
240 changes of molecular assemblies accompanying deprotonation. We discuss each of these below.

4.1 *Direct effects of deprotonation on chromophores: Substituted nitro-aromatics and phenols*

There is growing evidence that nitro-aromatic and substituted nitro-aromatic species are important chromophores in BrC[16] (and references therein), especially since they are some of only a few classes of molecules that absorb significantly into the visible region of the spectrum. The absorption spectra of substituted nitro-aromatic species tend to shift to longer wavelengths upon deprotonation[36] and could explain some of the apparent increased absorption at longer wavelengths. For example, we show in Figure S3 the absorption spectrum of 4-nitrocatechol with a peak at 350 nm at pH = 5 that decreases in intensity as pH is raised and is replaced by one at 425 nm at pH = 10. Such a shift, however, could only explain part of the observed change because nitrophenols are thought to account for only 4% of BrC absorption in ambient aerosols.[18,19] Even if they were to constitute a larger fraction of absorption, their behavior with changing pH is inconsistent with our observations. Specifically, there is no decrease in absorbance observed at shorter wavelengths as would be expected if such substituted nitro-aromatic species were replaced by their deprotonated analogs. What is more, these species generally don't absorb at wavelengths as long as 500 nm and therefore could not explain the increase in BrC absorption observed there. There would also need to be an unlikely coincidental superposition of many of these absorption spectra to account for the observed BrC spectra and their response to pH changes. So, while some of the pH dependence could be attributed to nitro-aromatic species, it is clear that other chromophores must contribute as well.

The difference absorption spectra (Figure 5) show a clear emergence of a peak near 300 nm as pH increases, which may correspond to the known absorption band of phenolate and alkyl-substituted phenolate anions in the 285 – 293 nm range.[57] What is more, this band appears at pH's in the range of pKa's reported for substituted phenols (4.7 – 11.6 [58]) and apparent pKa values attributed to phenolic groups in fulvic acids (7.2 – 10.9 [52]). It seems likely, given the existence of phenols and phenol groups in ambient aerosols,[13,16,54,55] biomass pyrolysis products,[59,60] and humic substances,[61,62] that some of the increase observed in the UV region of the spectra could be attributed to the conversion of phenols to

266 phenolate anions. However, the absorption increase at longer, visible wavelengths as well as at lower pH
267 values cannot be attributed directly to phenol deprotonation.[23]

268 It is also possible that phenolate anions formed at alkaline pH's contribute to increased visible absorption
269 through their participation in charge transfer complexes. [23] These complexes occur through a transfer of
270 charge from a donor group, such as a phenol, to an acceptor group, such as an aromatic carbonyl, and give
271 rise to electronic transitions with energies different than those of the transitions of the individual
272 constituent groups. Many different charge transfer complexes can be formed with a near-continuum of
273 transition energies, and there is evidence that they can account for a substantial fraction of the visible
274 absorption in both ambient particulate matter[20,21] and humic substances.[22,63] As pH increases, phenolate
275 anions, with lower ionization potentials than corresponding phenols[64], could act as better electron donors
276 giving rise to both stronger absorption bands as well as bands at longer wavelengths.[23] This effect,
277 however, cannot account for the observed increase in visible absorption at lower pH's (Figures 1 and 5)
278 where phenols are not deprotonated, though we do point out that deprotonation of substituted aromatic
279 carboxylic acids could play a role at lower pH values.

280 4.2 *Indirect effect of deprotonation on chromophores: Conformational changes*

281 There are many similarities, both chemical and optical, between WS BrC and humic substances.[30] Both
282 can contain molecules that are polyacidic with similar functional groups and moieties, including
283 polycyclic ring structures, hydroxyl, carboxyl, and carbonyl groups. They also each have absorption
284 spectra that are broad, featureless, and decrease in intensity with increasing wavelength, and they even
285 display similar fluorescence spectra.[21,30] These similarities suggest that they may share common chemical
286 explanations for the observed increase in absorption with pH, which they also both demonstrate. While
287 there have been relatively few studies investigating the effect of pH on BrC, there has been substantial
288 research on the effect that pH has on humic substances.

289 It is known is that humic substances appear to adopt smaller sizes at low pH, and this has been explained

in terms of a supramolecular assembly theory[49,65] in which small molecules form aggregates that are stabilized through a combination of hydrophobic forces and the formation of hydrogen bonds.[42] There is substantial evidence in the literature from size exclusion chromatography[66], fluorescence quenching,[67] TEM,[65] photon correlation spectroscopy,[65] small-angle X-ray scattering, [68] and NMR,[69] that humic and fulvic acids form such aggregates. It is also believed that as pH increases the anions created repel each other and hydrogen bonds are disrupted causing the assembly to adopt a more open configuration, which has been observed with a variety of methods, including diffusivity measurements,[27] small angle neutron scattering,[70] turbidity,[71] scanning electron microscopy,[71] and dynamic light scattering.[26,65,72-74]

Given the many similarities between ambient organic particulate matter and humic substances, we hypothesize that such conformational changes may be accompanying pH changes in ambient particulate matter as well. We suggest that the increased conformational flexibility at higher pH values can potentially influence the absorption spectrum in three ways: 1) decreased interaction between neighboring aromatic moieties making them absorb UV light more strongly, similar to the observed increase in absorption by DNA upon denaturation,[75] 2) increased flexibility of conjugated polyenes with longer extent of conjugation leading to greater absorption at longer wavelengths,[76] and 3) increased number and diversity of charge transfer contacts that can be made between donor moieties (e.g. phenols and phenolate ions) and acceptor moieties (e.g. aromatic ketones and aldehydes) increasing and red-shifting absorption.[20,23] In fact, such an alteration of "intrachromophore interactions" (e.g. charge transfer complexes) has been suggested by Janot et al.[51] to explain the observed increase in the broad absorption band of humic substances near 370 nm with increasing pH.

While all three of these effects may be important, interaction between aromatic moieties only affects the UV region of the spectrum and there is scant evidence for conjugated polyenes long enough to absorb visible light in aerosols. There is evidence for absorption by charge transfer complexes[20,21] in the UV and visible regions, however, and since these complexes are formed through local interactions between electron-donating and electron-accepting groups, it stands to reason that as pH changes these interactions

315 would be affected as well. Specifically, increasing pH could cause charge repulsion and hydrogen bond
316 disruption leading to a supramolecular assembly that is less conformationally constrained, which could
317 result in a larger number and greater diversity of charge transfer contacts. What is more, this change
318 could occur continuously over a wide range of pH's, beginning at acidic conditions where carboxylic acid
319 groups deprotonate (whose apparent pKa's in fulvic acids fall in the range 2 – 3.8 [52]) and extending to
320 alkaline conditions where phenols deprotonate (whose apparent pKa's in fulvic acids fall in the range 7.2
321 – 10.9 [52]).

322 Such an increase in conformational flexibility would also be expected to increase the likelihood of
323 forming all of the different charge transfer complexes with their different absorption bands. In fact, this is
324 exactly what is observed in the normalized difference absorption spectra (Figure 6a) at the longer
325 wavelengths (λ > 370 nm). Here, even as pH increases, the shape of the difference spectrum does not
326 change substantially. What is more, this region of the spectrum is precisely where Phillips and Smith
327 found charge transfer complexes in WS BrC to contribute the most to absorption, proportionately;[20] they
328 proposed a gradual transition from absorption dominated by independent chromophores at λ < 300 nm to
329 absorption dominated by charge transfer complexes at λ > 370 nm. That model is consistent with the
330 uniform spectral response observed in the normalized DAS spectra of Figure 6a if increasing pH affects
331 all of the near-continuum of charge transfer complexes in similar ways. Such a uniform behavior would
332 be highly coincidental for a superposition of chromophores and would be accompanied by a decrease in
333 absorption at shorter wavelengths (see Figure S3, for example), which is not observed.

334 4.3 *Atmospheric implications*

335 The systematic increase in absorbance accompanying increases in pH could have implications for the role
336 BrC plays in influencing the radiative balance in the atmosphere. For example, radiative forcing by
337 aerosols may be overestimated in climate models if refractive index values based on measurements made
338 at pH = 7 are used instead of those at lower values, such as pH = 2, which is more representative of
339 aerosols in the Southeastern U.S. Likewise, the climate impact may vary depending on season, location,

or particle age to the extent that pH changes with these conditions, too. To explore the potential effect of particle pH on radiative transfer, we have calculated the simple forcing efficiency (SFE, units of W/g) using the formulation of Chen and Bond,[6] (details given in Appendix 1 in the Supporting Information) which is commonly used to estimate climate impacts associated with changing particle properties.[8,77]

We investigated three possible scenarios involving a mixture of black carbon and organic matter (in a 1:10 mass ratio): 1) an external mixture consisting of separate black carbon and organic carbon particles, 2) an internal mixture consisting of particles containing a black carbon core coated with organic carbon, and 3) a combination of both internally mixed and externally mixed particles with 50% of the organic mass in each type of particle. For each of these, we set the value of the imaginary part of the refractive index, k_{OA} (550 nm), at pH = 2 to either 0.001 (low BrC absorption) or 0.010 (high BrC absorption). These values were chosen to represent a range of possible values for organic particulate material consistent with recent measurements, though we point out that substantial uncertainty remains regarding them.[8] And, since these values are used for all of the organic material, both BrC and non-absorbing, they are best thought of as effective refractive index values. The value of k_{OA} was parameterized as a function of both wavelength and pH based on the results of this study (details given in Appendix 2 in the Supporting Information).

Figure 7 shows the percentage increase in SFE calculated for the various scenarios as a function of pH. In all cases SFE increases with pH with the most pronounced effects occurring for completely externally mixed particles, which may be more representative of freshly emitted aerosols that haven't yet mixed internally. Such a case could represent newly formed aerosols near biomass burning sources, for example.[7] Clearly, the magnitude of the pH effect is influenced by the magnitude of absorption by the organic fraction, too. Thus, the influence of pH may be more pronounced in particles containing more highly absorbing, extremely low volatility organic compounds (ELVOC's) and thus might be a function of combustion conditions.[8] Figure 7 also illustrates that if pH is not accounted for in making bulk aerosol measurements, the impact of BrC absorption on SFE can be overestimated; for example, measurements

made at pH = 7 overestimate SFE by 5% - 49% (depending on k_{OA}(550 nm) and mixing state) compared to pH = 2, a value more representative of ambient aerosol in the Southeast U.S. based on thermodynamic modeling.[35] Thus, to the extent that aerosol pH may change in the atmosphere or may vary from sample to sample, its impact on aerosol absorption and radiative forcing should be considered.

Associated Content

Supporting Information

Details of simplified forcing efficiency calculations (Appendix 1); Details of parameterization of k_{OA} as a function of λ and pH (Appendix 2); Summary of samples (Table S1); MODIS fire count and HYSPLIT back trajectory map for sample impacted by wildfires, November 10, 2016 (Figure S1); Absorbance spectra of wildfire samples (Figure S2) and 4-nitrocatechol (Figure S3); Absorption Ångström exponent as a function of pH for all 10 baseline ambient samples (Figure S4). This material is available free of charge via the Internet at http://pubs.acs.org.

Author Information

Corresponding Author

*E-mail: gsmith@chem.uga.edu

Acknowledgments

The authors gratefully acknowledge support for this research by the National Science Foundation (AGS-1241621) and Prof. Rawad Saleh for providing Matlab code for performing the Mie calculations. The authors also gratefully acknowledge the NOAA Air Resources Laboratory (ARL) for the provision of the HYSPLIT transport and dispersion model and/or READY website (http://www.ready.noaa.gov) used in this publication.

389

390 **Table of Contents Graphic**

391 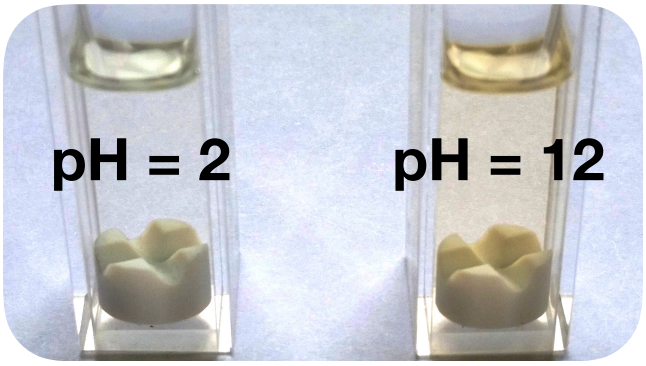

Figure Captions

Figure 1. Averaged absorbance spectra as a function of pH for the baseline ambient samples. Each spectrum is normalized to the value at 225 nm and pH = 11 for that sample. The linearity of the log-transformed spectra (inset) indicates quality of fit to a power law function.

Figure 2. Integrated absorbance (300-500 nm) normalized to values at pH = 2 as a function of pH. Baseline ambient samples separate into two groups (blue and green squares), one of which resembles the SRFA samples (gray triangles), while the other resembles the wildfire samples (orange circles).

Figure 3. Ratio of absorbance at pH = 5 (orange), pH = 7 (purple), and pH = 10 (green) relative to pH = 2 as a function of wavelength for: (a) baseline ambient samples, and (b) SRFA samples.

Figure 4. Absorption Ångström exponent as a function of pH for baseline ambient (blue squares) and SRFA (gray triangles) samples.

Figure 5. Average difference absorption spectra of baseline ambient samples for pH = 3-11 relative to pH = 2 displaying the emergence of spectral features near 260 nm and 300 nm as well as a long wavelength tail. Each sample was normalized to the value at 370 nm and pH = 11.

Figure 6. Normalized difference absorption spectra for pH = 3-11 relative to pH = 2 for (a) ambient and (b) SRFA samples. Each spectrum is normalized to the absorbance at 370 nm to allow relative changes in absorbance to be identified more clearly. Strikingly, the long wavelength tail ($\lambda > 370$ nm) is remarkably similar at all pH values and for both ambient and SRFA samples.

Figure 7. Calculated increase in estimated simple forcing efficiency (SFE) as a function of pH for weakly- and strongly-absorbing organic particulate matter (blue and red points, respectively). Three different mixing states with black carbon are assumed: externally mixed (circles), internally mixed (triangles), and 50:50 in which half the organic matter is internally mixed with black carbon and the other half is externally mixed.

References

(1) Bond, T. C.; Doherty, S. J.; Fahey, D. W.; Forster, P. M.; Berntsen, T.; DeAngelo, B. J.; Flanner, M. G.; Ghan, S.; Kaercher, B.; Koch, D.; et al. Bounding the role of black carbon in the climate system: A scientific assessment. *J. Geophys. Res.: Atmos.* **2013**, *118* (11), 5380–5552.

(2) Cheng, Y.; He, K.-B.; Du, Z.-Y.; Engling, G.; Liu, J.-M.; Ma, Y.-L.; Zheng, M.; Weber, R. The characteristics of brown carbon aerosol during winter in Beijing. *Atmos. Environ.* **2016**, *127*, 355–364.

(3) Hammer, M. S.; Martin, R. V.; van Donkelaar, A.; Buchard, V.; Torres, O.; Ridley, D. A.; Spurr, R. J. D. Interpreting the ultraviolet aerosol index observed with the OMI satellite instrument to understand absorption by organic aerosols: implications for atmospheric oxidation and direct radiative effects. *Atmos. Chem. Phys.* **2016**, *16* (4), 2507–2523.

(4) Kirchstetter, T. W.; Novakov, T.; Hobbs, P. Evidence that the spectral dependence of light absorption by aerosols is affected by organic carbon. *J. Geophys. Res.* **2004**, *109* (D21), D21208.

(5) Andreae, M. O.; Gelencser, A. Black carbon or brown carbon? The nature of light-absorbing carbonaceous aerosols. *Atmos. Chem. Phys.* **2006**, *6* (10), 3131–3148.

(6) Chen, Y.; Bond, T. C. Light absorption by organic carbon from wood combustion. *Atmos. Chem. Phys.* **2010**, *10* (4), 1773–1787.

(7) Lack, D. A.; Langridge, J. M.; Bahreini, R.; Cappa, C. D.; Middlebrook, A. M.; Schwarz, J. P. Brown carbon and internal mixing in biomass burning particles. *Proc. Natl. Acad. Sci. U. S. A.* **2012**, *109* (37), 14802–14807.

(8) Saleh, R.; Robinson, E. S.; Tkacik, D. S.; Ahern, A. T.; Liu, S.; Aiken, A. C.; Sullivan, R. C.; Presto, A. A.; Dubey, M. K.; Yokelson, R. J.; et al. Brownness of organics in aerosols from biomass burning linked to their black carbon content. *Nature Geosci.* **2014**, *7* (9), 647–650.

(9) Sareen, N.; Schwier, A.; Shapiro, E.; Mitroo, D.; McNeill, V. Secondary organic material formed by methylglyoxal in aqueous aerosol mimics. *Atmos. Chem. Phys.* **2010**, *10* (3), 997–1016.

(10) De Haan, D.; Tolbert, M.; Jimenez, J. L. Atmospheric condensed-phase reactions of glyoxal with methylamine. *Geophys. Res. Lett.* **2009**, *36* (11), L11819.

(11) Updyke, K. M.; Nguyen, T. B.; Nizkorodov, S. A. Formation of brown carbon via reactions of ammonia with secondary organic aerosols from biogenic and anthropogenic precursors. *Atmos. Environ.* **2012**, *63*, 22–31.

(12) Powelson, M. H.; Espelien, B. M.; Hawkins, L. N.; Galloway, M. M.; De Haan, D. O. Brown carbon formation by aqueous-phase carbonyl compound reactions with amines and ammonium sulfate. *Environ. Sci. Technol.* **2014**, *48* (2), 985–993.

(13) Lin, P.; Aiona, P. K.; Li, Y.; Shiraiwa, M.; Laskin, J.; Nizkorodov, S. A.; Laskin, A. Molecular characterization of brown carbon in biomass burning aerosol particles. *Environ. Sci. Technol.* **2016**, *50* (21), 11815–11824.

(14) Duporté, G.; Parshintsev, J.; Barreira, L. M. F.; Hartonen, K.; Kulmala, M.; Riekkola, M.-L. Nitrogen-Containing Low Volatile Compounds from Pinonaldehyde-Dimethylamine Reaction in the Atmosphere: A Laboratory and Field Study. *Environ. Sci. Technol.* **2016**, *50* (9), 4693–4700.

(15) Nguyen, T. B.; Laskin, A.; Laskin, J.; Nizkorodov, S. A. Brown carbon formation from ketoaldehydes of biogenic monoterpenes. *Faraday Discuss.* **2013**.

(16) Laskin, A.; Laskin, J.; Nizkorodov, S. A. Chemistry of atmospheric brown carbon. *Chem. Rev.* **2015**, *115* (10), 4335–4382.

(17) Desyaterik, Y.; Sun, Y.; Shen, X.; Lee, T.; Wang, X.; Wang, T.; Collett, J. L., Jr. Speciation of "brown" carbon in cloud water impacted by agricultural biomass burning in eastern China. *J. Geophys. Res.: Atmos.* **2013**, *118* (13), 7389–7399.

(18) Mohr, C.; Lopez-Hilfiker, F. D.; Zotter, P.; Prevot, A. S. H.; Xu, L.; Ng, N. L.; Herndon, S. C.; Williams, L. R.; Franklin, J. P.; Zahniser, M. S.; et al. Contribution of nitrated phenols to wood burning brown carbon light absorption in Detling, United Kingdom during winter time. *Environ. Sci. Technol.* **2013**, *47* (12), 6316–6324.

(19) Zhang, X.; Lin, Y.-H.; Surratt, J. D.; Weber, R. Sources, composition and absorption Ångström exponent of light-absorbing organic components in aerosol extracts from the Los Angeles Basin. *Environ. Sci. Technol.* **2013**, *47* (8), 3685–3693.

(20) Phillips, S. M.; Smith, G. D. Light absorption by charge transfer complexes in brown carbon aerosols.

Environ. Sci. Technol. **2014**, *1*, 382–386.
(21) Phillips, S. M.; Smith, G. D. Further evidence for charge transfer complexes in brown carbon aerosols from excitation-emission matrix fluorescence spectroscopy. *J. Phys. Chem. A* **2015**, *119* (19), 4545–4551.
(22) del Vecchio, R.; Blough, N. V. On the origin of the optical properties of humic substances. *Environ. Sci. Technol.* **2004**, *38* (14), 3885–3891.
(23) Sharpless, C. M.; Blough, N. V. The importance of charge-transfer interactions in determining chromophoric dissolved organic matter (CDOM) optical and photochemical properties. *Environ. Sci. Process. Impacts* **2014**, *16* (4), 654–671.
(24) Ghosh, K.; Schnitzer, M. UV and visible absorption spectroscopic investigations in relation to macromolecular characteristics of humic substances. *J. Soil. Sci.* **1979**, *30* (4), 735–745.
(25) Baes, A. U.; Bloom, P. R. Fulvic-acid ultraviolet-visible spectra - Influence of solvent and pH. *Soil Sci. Soc. Am. J.* **1990**, *54* (5), 1248–1254.
(26) Pinheiro, J. P.; Mota, A. M.; d'Oliveira, J. M. R.; Martinho, J. M. G. Dynamic properties of humic matter by dynamic light scattering and voltammetry. *Anal. Chim. Acta* **1996**, *329* (1-2), 15–24.
(27) Wang, Y.; Combe, C.; Clark, M. M. The effects of pH and calcium on the diffusion coefficient of humic acid. *J. Membrane Sci.* **2001**, *183* (1), 49–60.
(28) Brigante, M.; Zanini, G.; Avena, M. On the dissolution kinetics of humic acid particles - Effects of pH, temperature and Ca^{2+} concentration. *Colloid Surf. A* **2007**, *294* (1-3), 64–70.
(29) Dryer, D. J.; Korshin, G. V.; Fabbricino, M. In situ examination of the protonation behavior of fulvic acids using differential absorbance spectroscopy. *Environ. Sci. Technol.* **2008**, *42* (17), 6644–6649.
(30) Graber, E. R.; Rudich, Y. Atmospheric HULIS: How humic-like are they? A comprehensive and critical review. *Atmos. Chem. Phys.* **2006**, *6* (3), 729–753.
(31) Fridlind, A. M.; Jacobson, M. Z. A study of gas–aerosol equilibrium and aerosol pH in the remote marine boundary layer during the First Aerosol Characterization Experiment (ACE 1). *J. Geophys. Res. - Atmos.* **2000**, *105* (D13), 17325–17340.
(32) Keene, W. C.; Pszenny, A.; Maben, J. R.; Sander, R. Variation of marine aerosol acidity with particle size. *Geophys. Res. Lett.* **2002**, *29* (7), 1101.
(33) Pszenny, A. A. P.; Moldanová, J.; Keene, W. C.; Sander, R.; Maben, J. R.; Martinez, M.; Crutzen, P. J.; Perner, D.; Prinn, R. G. Halogen cycling and aerosol pH in the Hawaiian marine boundary layer. *Atmos. Chem. Phys.* **2004**, *4* (1), 147–168.
(34) Guo, H.; Xu, L.; Bougiatioti, A.; Cerully, K. M.; Capps, S. L.; Hite, J. R., Jr; Carlton, A. G.; Lee, S. H.; Bergin, M. H.; Ng, N. L.; et al. Fine-particle water and pH in the southeastern United States. *Atmos. Chem. Phys.* **2015**, *15* (9), 5211–5228.
(35) Weber, R.; Guo, H.; Russell, A. G.; Nenes, A. High aerosol acidity despite declining atmospheric sulfate concentrations over the past 15 years. *Nature Geosci.* **2016**, *9* (4), 282–286.
(36) Lee, H. J. J.; Aiona, P. K.; Laskin, A.; Laskin, J.; Nizkorodov, S. A. Effect of solar radiation on the optical properties and molecular composition of laboratory proxies of atmospheric brown carbon. *Environ. Sci. Technol.* **2014**, *48* (17), 10217–10226.
(37) Teich, M.; Pinxteren, D. V.; Wang, M.; Kecorius, S.; Wang, Z.; Müller, T.; Močnik, G.; Herrmann, H. Contributions of nitrated aromatic compounds to the light absorption of water-soluble and particulate brown carbon in different atmospheric environments in Germany and China. *Atmos. Chem. Phys.* **2017**, *17* (3), 1653–1672.
(38) Ahillen, S. Forest fires burn 119,000 acres in 8 Southeastern states. *USA Today*. November 20, 2016.
(39) NASA. NASA EOSDIS Worldview. *https://earthdata.nasa.gov/worldview*.
(40) Stein, A. F.; Draxler, R. R.; Rolph, G. D. NOAA's HYSPLIT atmospheric transport and dispersion modeling system. *Bull. Amer. Meteor. Soc.* **2015**, *96*, 2059–2077.
(41) Hecobian, A.; Zhang, X.; Zheng, M.; Frank, N.; Edgerton, E. S.; Weber, R. Water-soluble organic aerosol material and the light-absorption characteristics of aqueous extracts measured over the Southeastern United States. *Atmos. Chem. Phys.* **2010**, *10* (13), 5965–5977.
(42) Davis, H.; Mott, C. J. B. Titrations of fulvic acid fractions I: interactions influencing the dissociation/reprotonation equilibria. *J. Soil. Sci.* **1981**, *32* (3), 379–391.
(43) Marshall, S. J.; Young, S. D.; Gregson, K. Humic acid–proton equilibria: A comparison of two models and assessment of titration error. *J. Soil. Sci.* **1995**, *46* (3), 471–480.
(44) Heighton, L. P.; Schmidt, W. F. Probing the pH dependent optical properties of aquatic, terrestrial and microbial humic substances by sodium borohydride reduction. *J. Geo. Geo.* **2014**, *6* (3), 214.

(45) Schendorf, T. M. Effect of borohydride reduction and pH on the optical properties of humic substances. M.S. Dissertation, University of Maryland, College Park, MD, 2014.
(46) Claeys, M.; Vermeylen, R.; Yasmeen, F.; Gómez-González, Y.; Chi, X.; Maenhaut, W.; Mészáros, T.; Salma, I. Chemical characterisation of humic-like substances from urban, rural and tropical biomass burning environments using liquid chromatography with UV/vis photodiode array detection and electrospray ionisation mass spectrometry. *Environ. Chem.* **2012**, *9* (3), 273–284.
(47) Lin, P.; Laskin, J.; Nizkorodov, S. A.; Laskin, A. Revealing Brown Carbon Chromophores Produced in Reactions of Methylglyoxal with Ammonium Sulfate. *Environ. Sci. Technol.* **2015**, *49* (24), 14257–14266.
(48) Avdeef, A.; Sofen, S. R.; Bregante, T. L.; Raymond, K. N. Coordination chemistry of microbial iron transport compounds. 9. Stability constants for catechol models of enterobactin. *J. Am. Chem. Soc.* **1978**, *100* (17), 5362–5370.
(49) Piccolo, A. The supramolecular structure of humic substances. *Soil Sci.* **2001**, *166* (11), 810–832.
(50) Sutton, R.; Sposito, G. Molecular structure in soil humic substances: The new view. *Environ. Sci. Technol.* **2005**, *39* (23), 9009–9015.
(51) Janot, N.; Reiller, P. E.; Korshin, G. V.; Benedetti, M. F. Using spectrophotometric titrations to characterize humic acid reactivity at environmental concentrations. *Environ. Sci. Technol.* **2010**, *44* (17), 6782–6788.
(52) Milne, C. J.; Kinniburgh, D. G.; Tipping, E. Generic NICA-Donnan model parameters for proton binding by humic substances. *Environ. Sci. Technol.* **2001**, *35* (10), 2049–2059.
(53) Russell, L. M.; Bahadur, R.; Ziemann, P. J. Identifying organic aerosol sources by comparing functional group composition in chamber and atmospheric particles. *Proc. Natl. Acad. Sci. U. S. A.* **2011**, *108* (9), 3516–3521.
(54) Havers, N.; Burba, P.; Lambert, J.; Klockow, D. Spectroscopic characterization of humic-like substances in airborne particulate matter. *J. Atmos. Chem.* **1998**, *29* (1), 45–54.
(55) Bahadur, R.; Uplinger, T.; Russell, L. M.; Sive, B. C.; Cliff, S. S.; Millet, D. B.; Goldstein, A.; Bates, T. S. Phenol groups in northeastern U.S. submicrometer aerosol particles produced from seawater sources. *Environ. Sci. Technol.* **2010**, *44* (7), 2542–2548.
(56) Calvert, J. G.; Pitts, J. N. *Photochemistry*; John Wiley & Sons, Inc.: New York, 1966.
(57) Dearden, J. C.; Forbes, W. F. Light absorption studies: Part XIV. The ultraviolet absorption spectra of phenols. *Can. J. Chemistry* **1959**, *37*, 1294–1304.
(58) Li, C.; Hoffman, M. Z. One-electron redox potentials of phenols in aqueous solution. *J. Phys. Chem. B* **1999**, *103* (32), 6653–6656.
(59) Achladas, G. E. Analysis of biomass pyrolysis liquids: separation and characterization of phenols. *J. Chromatogr. A* **1991**, *542*, 263–275.
(60) Simoneit, B.; Rogge, W.; Mazurek, M.; Standley, L.; Hildemann, L.; Cass, G. Lignin pyrolysis products, lignans, and resin acids as specific tracers of plant classes in emissions from biomass combustion. *Environ. Sci. Technol.* **1993**, *27* (12), 2533–2541.
(61) Andjelkovic, T.; Perovic, J.; Purenovic, M.; Blagojevic, S.; Nikolic, R.; Andjelkovic, D.; Bojic, A. A direct potentiometric titration study of the dissociation of humic acid with selectively blocked functional groups. *Eclét. Quim.* **2006**, *31* (3), 39–46.
(62) Boyle, E. S.; Guerriero, N.; Thiallet, A.; del Vecchio, R.; Blough, N. V. Optical properties of humic substances and cdom: Relation to structure. *Environ. Sci. Technol.* **2009**, *43* (7), 2262–2268.
(63) Ma, J.; del Vecchio, R.; Golanoski, K. S.; Boyle, E. S.; Blough, N. V. Optical properties of humic substances and cdom: Effects of borohydride reduction. *Environ. Sci. Technol.* **2010**, *44* (14), 5395–5402.
(64) Ghosh, D.; Roy, A.; Seidel, R.; Winter, B.; Bradforth, S.; Krylov, A. I. First-principle protocol for calculating ionization energies and redox potentials of solvated molecules and ions: Theory and application to aqueous phenol and phenolate. *J. Phys. Chem. B* **2012**, *116* (24), 7269–7280.
(65) Baalousha, M.; Motelica-Heino, M.; Coustumer, P. L. Conformation and size of humic substances: Effects of major cation concentration and type, pH, salinity, and residence time. *Colloid Surf. A* **2006**, *272* (1-2), 48–55.
(66) Conte, P.; Piccolo, A. Conformational arrangement of dissolved humic substances. Influence of solution composition on association of humic molecules. *Environ. Sci. Technol.* **1999**, No. 33, 1682–1690.
(67) Kumke, M. U.; Lohmannsroben, H. G.; Roch, T. Fluorescence quenching of polycyclic aromatic-compounds by humic-acid. *Analyst* **1994**, *119* (5), 997–1001.
(68) Pranzas, P. K.; Willumeit, R.; Gehrke, R.; Thieme, J.; Knöchel, A. Characterisation of structure and aggregation processes of aquatic humic substances using small-angle scattering and X-ray microscopy.

Anal. Bioanal. Chem. **2003**, *376* (5), 618–625.
(69) Simpson, A. J.; Kingery, W. L.; Hayes, M. H.; Spraul, M.; Humpfer, E.; Dvortsak, P.; Kerssebaum, R.; Godejohann, M.; Hofmann, M. Molecular structures and associations of humic substances in the terrestrial environment. *Naturwissenschaften* **2002**, *89* (2), 84–88.
(70) Diallo, M. S.; Glinka, C. J.; Goddard, W. A.; Johnson, J. H. Characterization of nanoparticles and colloids in aquatic systems 1. small angle neutron scattering investigations of suwannee river fulvic acid aggregates in aqueous solutions. *J. Nanopart. Res.* **2005**, *7* (4-5), 435–448.
(71) Senesi, N.; Rizzi, F. R.; Dellino, P.; Acquafredda, P. Fractal dimension of humic acids in aqueous suspension as a function of ph and time. *Soil Sci. Soc. Am. J.* **1996**, *60* (6), 1773–1780.
(72) Alvarez-Puebla, R. A.; Garrido, J. J. Effect of pH on the aggregation of a gray humic acid in colloidal and solid states. *Chemosphere* **2005**, *59* (5), 659–667.
(73) Jovanović, U. D.; Marković, M. M.; Cupać, S. B.; Tomić, Z. P. Soil humic acid aggregation by dynamic light scattering and laser Doppler electrophoresis. *J. Plant Nutr. Soil Sc.* **2013**, *176* (5), 674–679.
(74) Guo, R.; Ma, J. Reduction-induced molecular signature of humic substances: Structural evidence for optical changes. *RSC Adv.* **2014**, *4* (49), 25880–25885.
(75) D'Abramo, M.; Castellazzi, C. L.; Orozco, M.; Amadei, A. On the nature of DNA hyperchromic effect. *J. Phys. Chem. B* **2013**, *117* (29), 8697–8704.
(76) Kohler, B.; Woehl, J. A simple-model for conjugation lengths in long polyene chains. *J. Chem. Phys.* **1995**, *103* (14), 6253–6256.
(77) Erlick, C.; Abbatt, J.; Rudich, Y. How Different Calculations of the Refractive Index Affect Estimates of the Radiative Forcing Efficiency of Ammonium Sulfate Aerosols. *J. Atmos. Sci.* **2011**, *68* (9), 1845–1852.

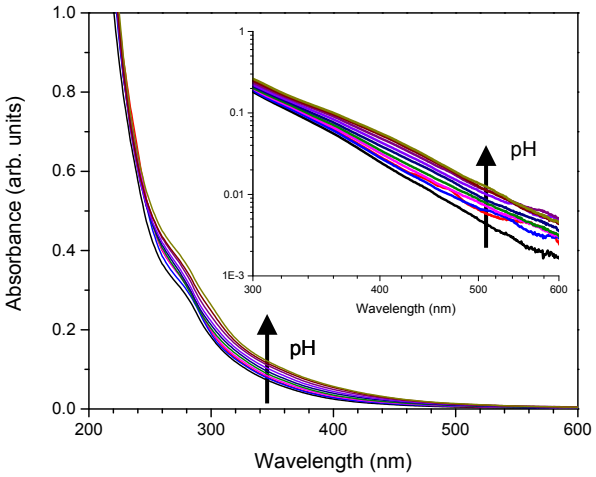

Figure 1.

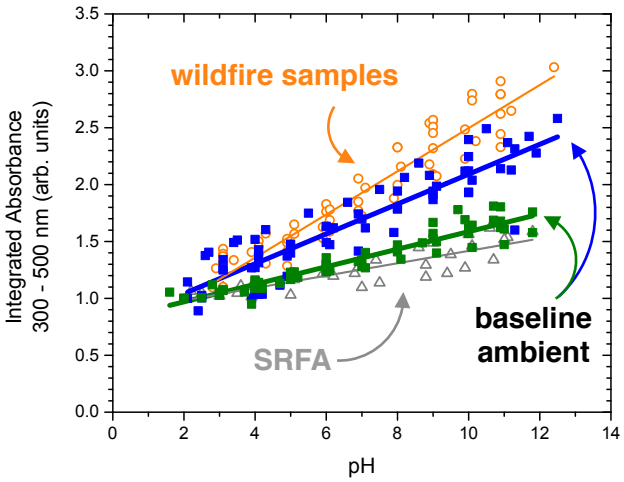
wildfire samples
baseline
ambient
SRFA
Integrated Absorbance
300 - 500 nm (arb. units)
pH
0.0
0.5
1.0
1.5
2.0
2.5
3.0
3.5
0
2
4
6
8
10
12
14

Figure 2.

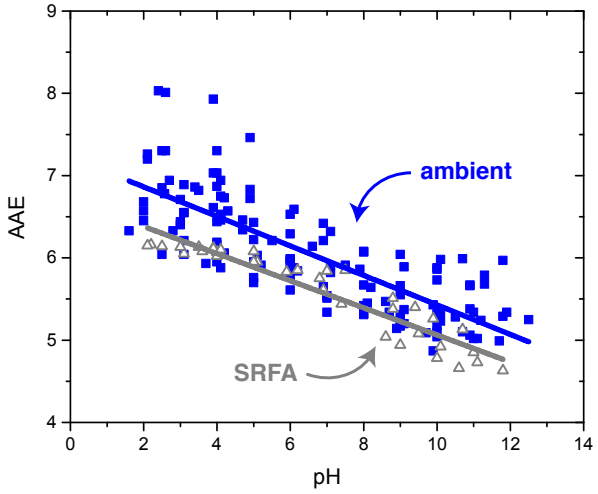

Figure 4.

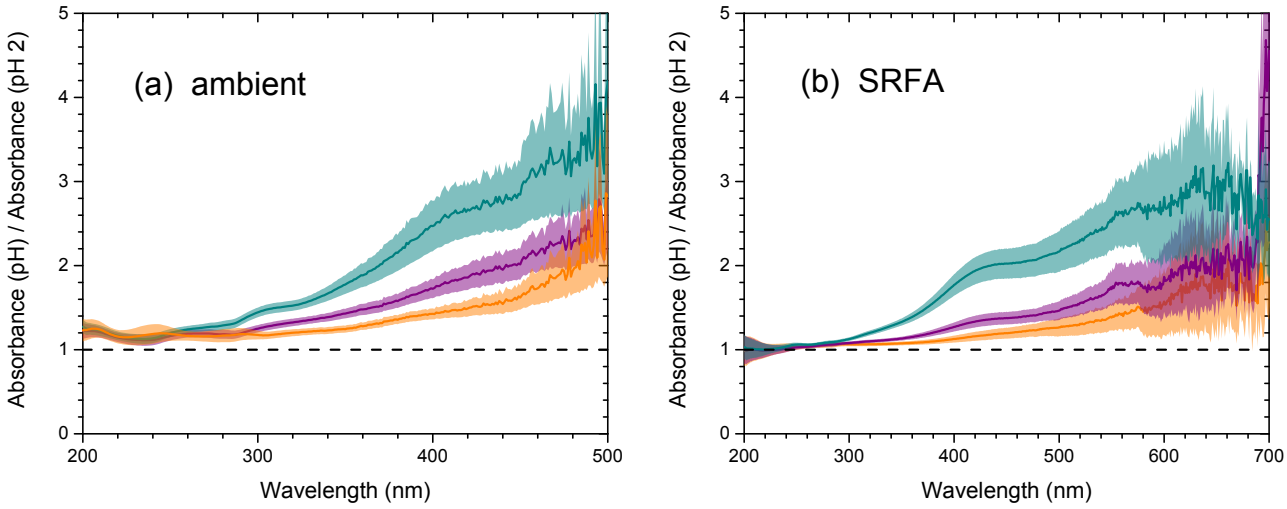
(a) ambient
(b) SRFA
Absorbance (pH) / Absorbance (pH 2)
Wavelength (nm)
0
1
2
3
4
5
200
300
400
500
600
700

Figure 3.

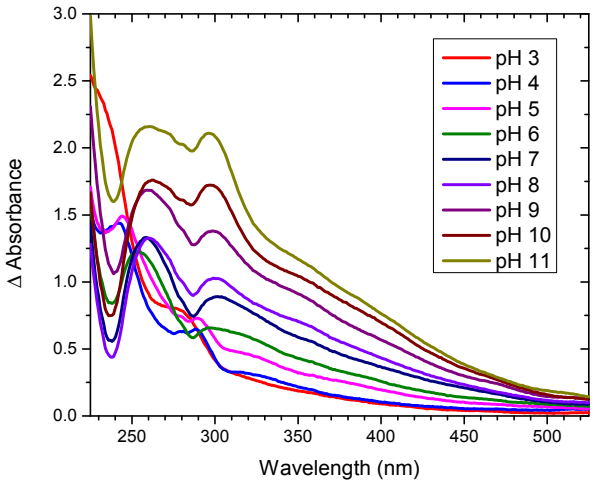
3.0
2.5
2.0
1.5
1.0
0.5
0.0
Δ Absorbance
250
300
350
400
450
500
Wavelength (nm)
pH 3
pH 4
pH 5
pH 6
pH 7
pH 8
pH 9
pH 10
pH 11

Figure 5.

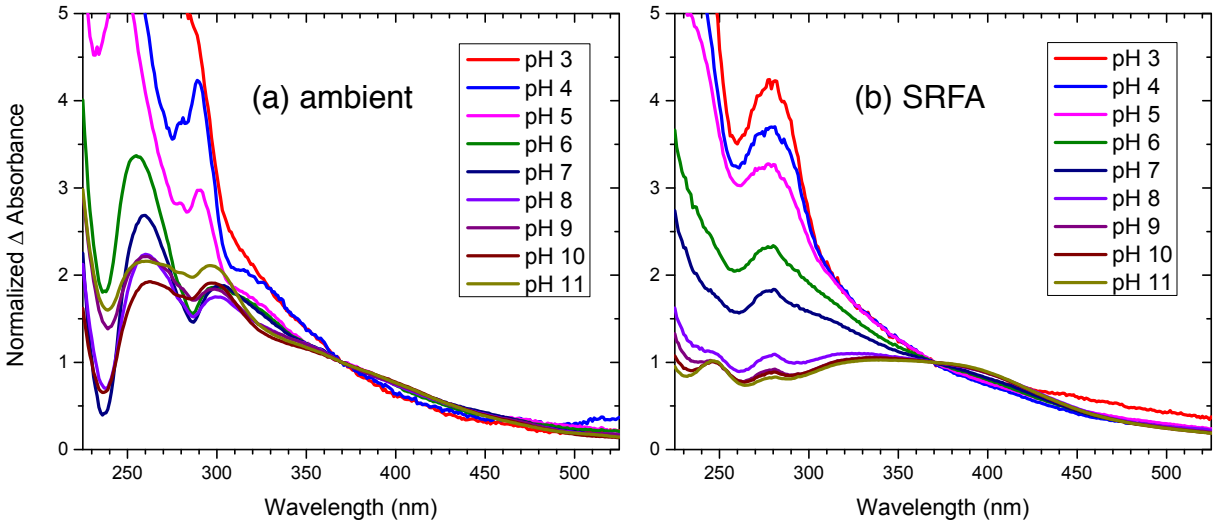
(a) ambient
(b) SRFA
pH 3
pH 4
pH 5
pH 6
pH 7
pH 8
pH 9
pH 10
pH 11
Normalized Δ Absorbance
Wavelength (nm)
0
1
2
3
4
5
250
300
350
400
450
500

Figure 6.

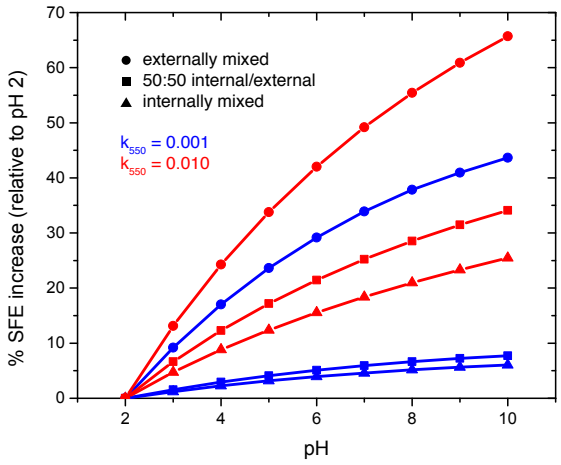
% SFE increase (relative to pH 2)
pH
externally mixed
50:50 internal/external
internally mixed
k550 = 0.001
k550 = 0.010
0
10
20
30
40
50
60
70
2
4
6
8
10

Figure 7.

Supporting Information for

Light absorption by brown carbon in the Southeastern United States is pH dependent

Sabrina M. Phillips, Aleia D. Bellcross, Geoffrey D. Smith*

Department of Chemistry, University of Georgia, 140 Cedar St. Athens, GA 30602 USA

*gsmith@chem.uga.edu, to whom correspondence should be addressed.

9 pages:

Appendix 1. Details of simplified forcing efficiency (SFE) calculations.

Appendix 2. Details of the parameterization of k_{OA} as a function of λ and pH.

Table S1. Summary of all samples.

Figure S1. Overlayed MODIS fire counts and HYSPLIT back trajectory calculations for November 10, 2016 sample.

Figure S2. Absorbance spectra of ambient Athens, GA samples affected by wildfires (November, 2016).

Figure S3. Absorbance spectra of a 50 mg/L aqueous 4-nitrocatechol solution at pH = 5, pH = 7, and pH = 10.

Figure S4. Absorption Ångström exponent (AAE) as a function of pH for individual baseline ambient Athens, GA filter samples.

Appendix 1. Details of the simplified forcing efficiency (SFE) calculations.

The SFE was calculated at each pH value and mixing state according to the formulation of Chen and Bond[1]:

$$SFE = \int_{300nm}^{800nm} \frac{dSFE}{d\lambda} = \int_{300nm}^{800nm} -\frac{1}{4}\frac{dS}{d\lambda}\tau_{atm}^{2}\left(1-F_c\right)\left[2\left(1-a_s\right)^{2}\bullet\beta\bullet MSC - 4a_s\bullet MAC\right] \quad \text{(S1)}$$

where a_s is the solar irradiance (taken from the ASTM G173-03 reference spectrum,[2] τ_{atm} is the atmospheric transmission (0.79 [3]), F_c is the cloud fraction (0.6 [3]), and a_s is the surface albedo (0.19 [3]). The backscatter fraction, β, is taken to be a constant value (0.17 [4]) at all wavelengths and for all particle diameters, and MSC and MAC are the mass scattering and mass absorption cross section of the particles, respectively. The MSC and MAC are calculated from Mie theory for coated spheres consisting of both black carbon and organic material. The value of k_{OA} was parameterized as a function of both wavelength and pH based on the results of this study (see Appendix 2).

Appendix 2. Details of the parameterization of k_{OA} as a function of λ and pH.

The imaginary part of the refractive index for the organic aerosol component, k_{OA}, was parameterized as a function of both λ and pH according to the findings of the present work.

The wavelength dependence of the value of k_{OA} was assumed to follow a power law function:

$$k_{OA}(\lambda, pH) = k_{550}(pH) \cdot \left(\frac{550}{pH} \right)^{w(pH)} \quad \text{(S2)}$$

with k_{550} the value of k_{OA} at λ = 550 nm and the exponent, w, describing the wavelength dependence. Both k_{550} and w are functions of pH:

$$k_{550}(pH) = k_{550}(pH = 2) \cdot \left[1 + 0.25 \cdot (pH - 2) \right] \quad \text{(S3)}$$

which is derived from the spectra shown in Figure 1 in the main text, and:

$$w(pH) = 6.16 - 0.17 \cdot pH \quad \text{(S4)}$$

which is derived from the observed trend of AAE vs. pH (Figure 4 in the main text) and the assumption that w = AAE - 1.[4]

Table S1. Summary of all samples collected and analyzed.

Date (2016)	Hours collected	Initial pH	AAE at pH7	Air mass source direction	Visibility (miles)
9/22-9/29	168	3.9	6.21	WNW	9
10/16-10/17	24	4	6.32	SE	9
9/29-9/30	24	4.9	6.42	NW	10
8/9-8/15	144	3.7	5.54	S	9.4
10/14-10/16	48	4.2	5.34	ENE	8.3
10/28-11/2	120	4.1	5.82	ENE	9
11/2-11/4	48	4.7	5.65	NW	7
4/27-4/30	72	4.2	5.51	WSW	9.5
10/17-10/18	24	4.1	6.02	SW	10
10/31-11/02	48		5.9	ENE	8
11/8-11/10	*47.5*	*4.9*	*N/A*	*N*	*8.6*
11/10-11/11	*24*	*4.3*	*N/A*	*NW*	*3.8*
11/11	*7*	*4.9*	*N/A*	*NW*	*3.8*
11/14-11/15	*25*		*N/A*	*WNW*	*2*
11/15-11/16	*24.5*	*4.1*	*N/A*	*NW*	*4*

Samples classified as “wildfire” samples from MODIS fire counts and HYSPLIT back trajectory calculations are indicated in italics. Air mass source direction was determined from HYSPLIT back trajectory calculations. Visibility was taken from https:/www.wunderground.com.

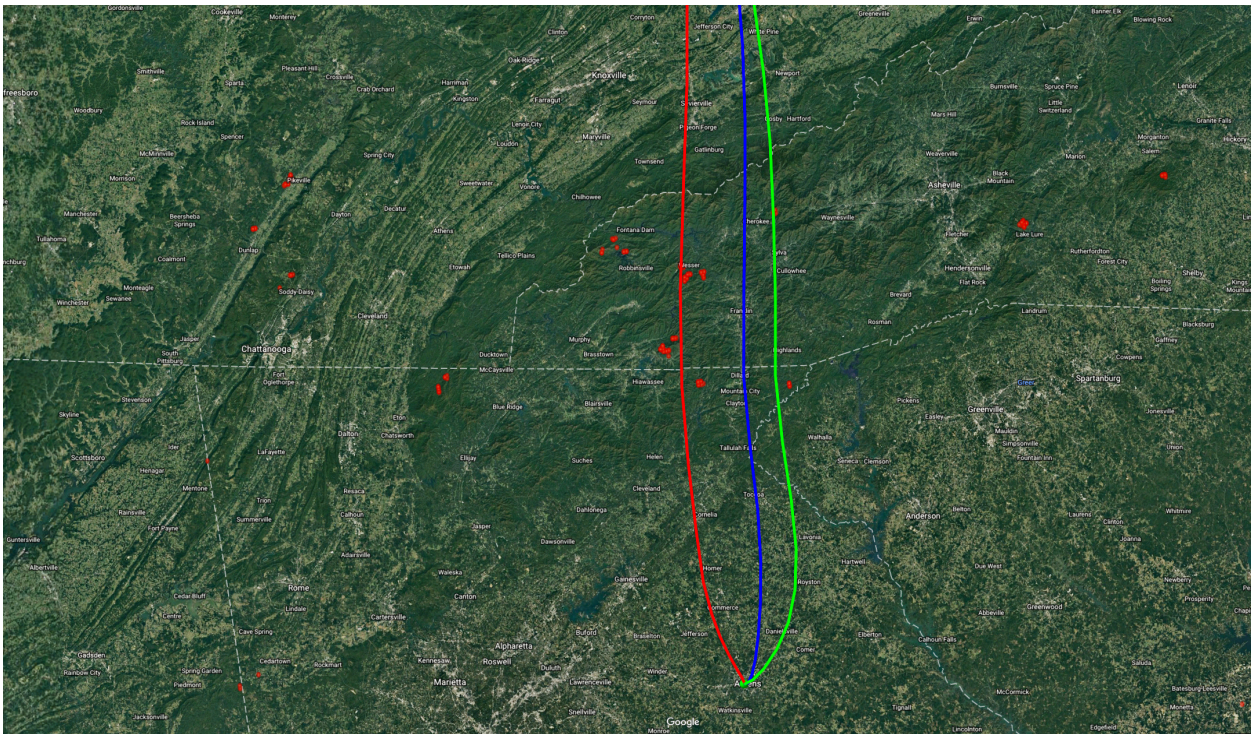

Figure S1. Map of overlaid MODIS fire counts (red dots) and calculated HYSPLIT back trajectories (50 m, red line; 250 m, blue line; 500 m, green line) for air mass sampled at Athens, GA on November 10, 2016. The other designated wildfire samples also show sampled air masses traveled through regions impacted by wildfires. (Map data: Google, IBCAO Data SIO, NOAA, U.S. Navy, NGA, GEBCO Landsat/Copernicus).

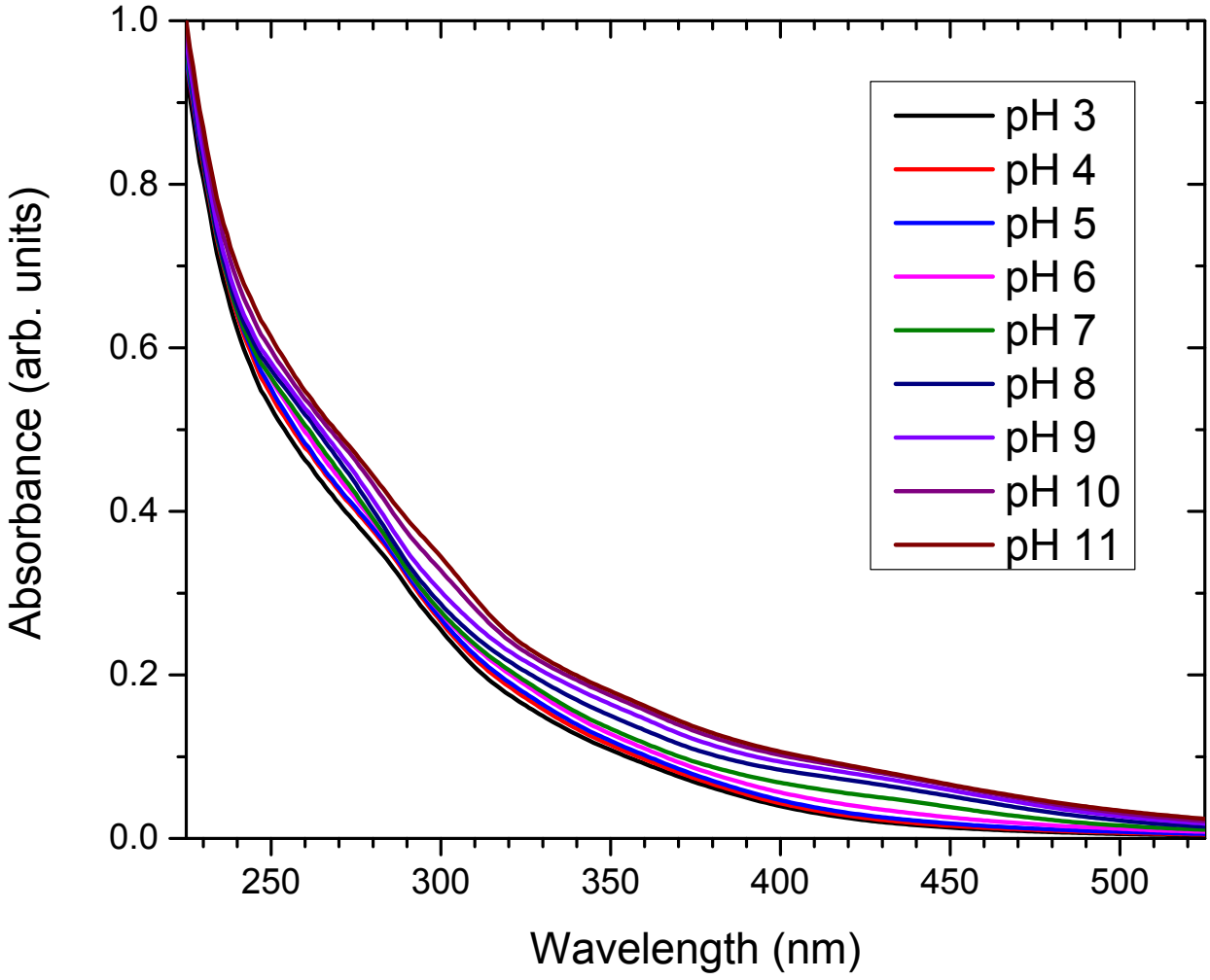

Figure S2. Averaged absorbance spectra of ambient Athens, GA samples affected by wildfires (November, 2016). The spectra are not fit by a power law function as well as the baseline ambient spectra are.

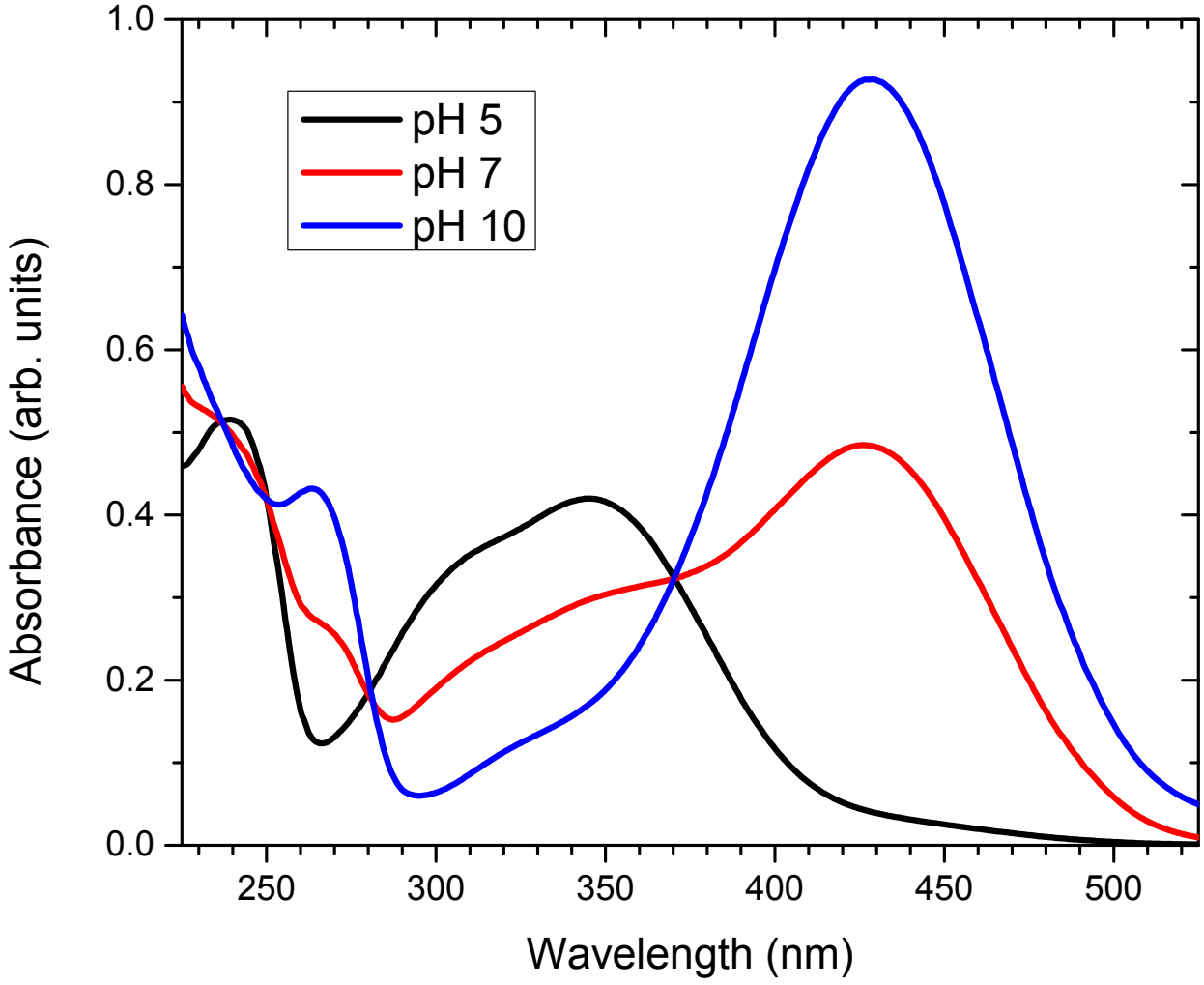

Figure S3. Absorbance spectra of a 50 mg/L aqueous 4-nitrocatechol solution at pH = 5, pH = 7, and pH = 10. The peak at 430 nm present at pH =7 and pH = 10 corresponds to the deprotonated phenolate form.

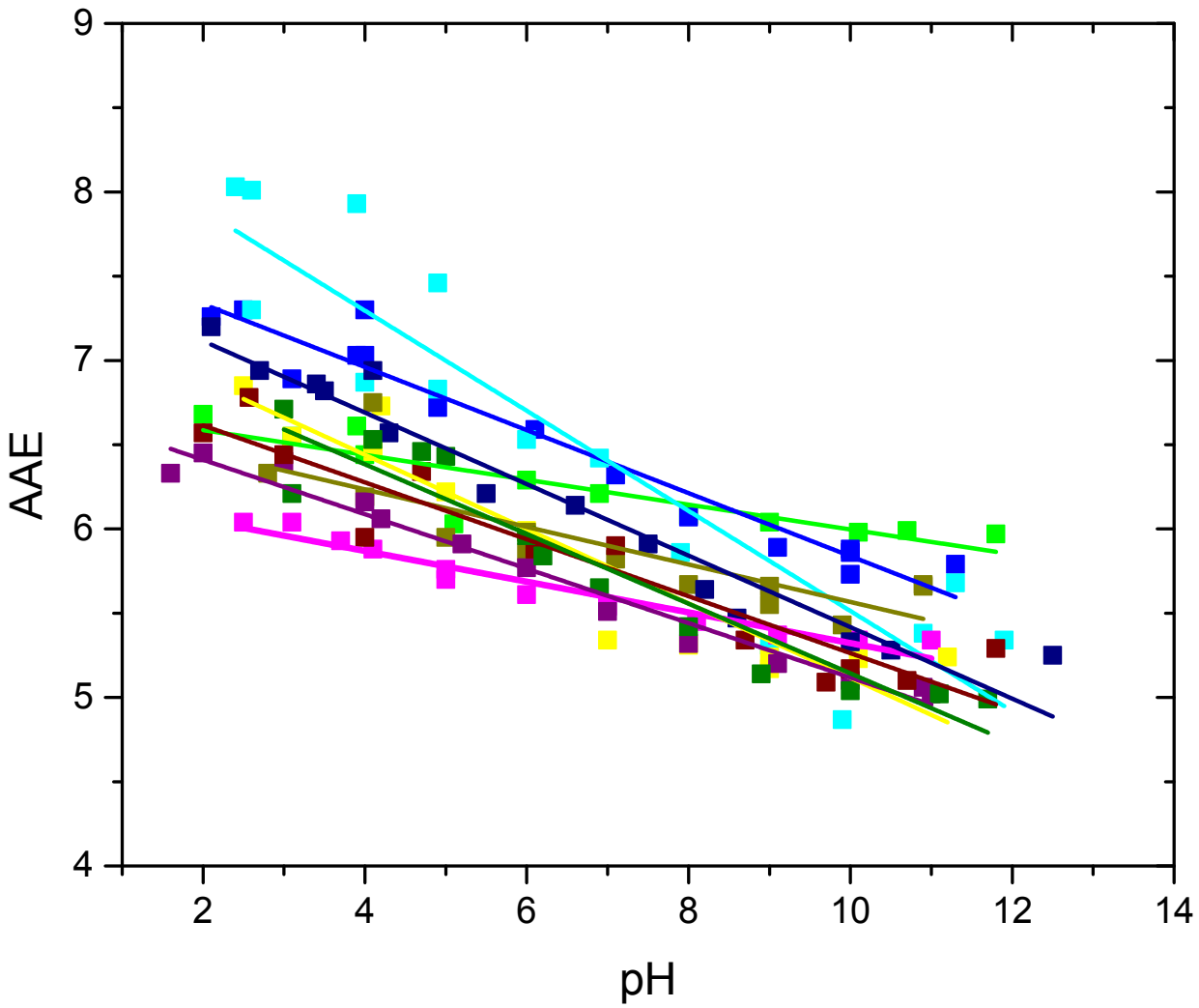

Figure S4. Absorption Ångström exponent (AAE) as a function of pH for individual baseline ambient Athens, GA filter samples. All samples show a similar trend of decreasing AAE with increasing pH.

References

(1) Chen, Y.; Bond, T. C. Light Absorption by Organic Carbon From Wood Combustion. Atmos. Chem. Phys. 2010, 10, 1773–1787.

(2) ASTM G173-03(2012), Standard Tables for Reference Solar Spectral Irradiances: Direct Normal and Hemispherical on 37° Tilted Surface; ASTM International: West Conshohocken, PA, 2012.

(3) Chylek, P.; Wong, J. Effect of Absorbing Aerosols on Global Radiation Budget. Geophys. Res. Lett. 1995, 22, 929–931.

(4) Saleh, R.; Robinson, E. S.; Tkacik, D. S.; Ahern, A. T.; Liu, S.; Aiken, A. C.; Sullivan, R. C.; Presto, A. A.; Dubey, M. K.; Yokelson, R. J.; et al. Brownness of Organics in Aerosols From Biomass Burning Linked to Their Black Carbon Content. Nature Geosci. 2014, 7, 647–650.